The energy dependence of the $pp \to K^+n\Sigma^+$ reaction close to threshold

Yu. Valdau,[1,2,*] S. Barsov,[1] M. Büscher,[2] D. Chiladze,[2,3] S. Dymov,[4,5] A. Dzyuba,[1] M. Hartmann,[2] A. Kacharava,[2] I. Keshelashvili,[6,3] A. Khoukaz,[7] V. Koptev,[1] P. Kulessa,[8] S. Merzliakov,[5,2] M. Mielke,[7] S. Mikirtychiants,[1,2] M. Nekipelov,[2] H. Ohm,[2] M. Papenbrock,[7] F. Rathmann,[2] V. Serdyuk,[5,2] H. Ströher,[2] S. Trusov,[9,10] and C. Wilkin[11]

[1]*High Energy Physics Department, Petersburg Nuclear Physics Institute, RU-188350 Gatchina, Russia*
[2]*Institut für Kernphysik and Jülich Centre for Hadron Physics, Forschungszentrum Jülich, D-52425 Jülich, Germany*
[3]*High Energy Physics Institute, Tbilisi State University, 0186 Tbilisi, Georgia*
[4]*Physikalisches Institut II, Universität Erlangen-Nürnberg, D-91058 Erlangen, Germany*
[5]*Laboratory of Nuclear Problems, JINR, RU-141980 Dubna, Russia*
[6]*Physics Dept., University of Basel, Klingelbergstrasse 82, CH-4056 Basel, Switzerland*
[7]*Institut für Kernphysik, Universität Münster, D-48149 Münster, Germany*
[8]*H. Niewodniczanski Institute of Nuclear Physics PAN, PL-31342 Cracow, Poland*
[9]*Institut für Kern- und Hadronenphysik, Forschungszentrum Rossendorf, D-01314 Dresden, Germany*
[10]*Skobeltsyn Institute of Nuclear Physics, Lomonosov Moscow State University, RU-119991 Moscow, Russia*
[11]*Physics and Astronomy Department, UCL, London WC1E 6BT, United Kingdom*

(Dated: December 15, 2013)

The production of the Σ^+ hyperon through the $pp \to K^+n\Sigma^+$ reaction has been investigated at four energies close to threshold, 1.826, 1.920, 1.958, and 2.020 GeV. At low energies, correlated $K^+\pi^+$ pairs can only originate from Σ^+ production so that their measurement allows the total cross section for the reaction to be determined. The results obtained are completely consistent with the values extracted from the study of the K^+-proton correlation spectra obtained in the same experiment. These spectra, as well as the inclusive K^+ momentum distributions, also provide conservative upper limits on the Σ^+ production rates. The measurements show a Σ^+ production cross section that varies roughly like phase space and, in particular, none of the three experimental approaches used supports the anomalously high near-threshold $pp \to K^+n\Sigma^+$ total cross section previously reported [T. Rożek *et al.*, Phys. Lett. B **643**, 251 (2006)].

PACS numbers: 13.75.-n, 14.20.Jn, 14.40.Aq, 25.40.Ve

I. INTRODUCTION

The energy dependence of the total cross section for associated strangeness production in the exclusive $pp \to K^+p\Lambda$ reaction near threshold has been investigated in a series of experiments undertaken at the COSY accelerator of the Forschungszentrum Jülich using the COSY-11 and COSY-TOF detectors [1–6]. The resulting behavior can be described in terms of a three-body phase space that is influenced by a strong final state interaction (FSI) between the Λ hyperon and the emerging proton.

The situation for Σ^0 production in the analogous $pp \to K^+p\Sigma^0$ reaction is rather different since the existing data show a total cross section that varies as expected from three-body phase space, with no evidence for a strong $\Sigma^0 p$ FSI [3, 5, 7]. A second distinction between the production of the two hyperons in proton-proton collisions is that, at the same value of the excess energy ε close to threshold, the total cross section for $pp \to K^+p\Sigma^0$ is at least one order of magnitude less than that of $pp \to K^+p\Lambda$. This probably reflects differences in the underlying reaction mechanisms as well as between the two FSI involved.

Since the Σ has isospin $I = 1$, extra light may be cast on both the FSI and reaction mechanism questions through the study of Σ^+ production in the $pp \to K^+n\Sigma^+$ reaction. The first measurements on this channel were completed by the COSY-11 collaboration at proton beam energies of $T_p = 1.826$ GeV and 1.958 GeV, *i.e.*, at $\varepsilon = 13$ MeV and 60 MeV, by detecting the neutron in coincidence with the produced K^+ [8]. The values obtained for the total cross section were strikingly high compared to those for Σ^0 production, or indeed with those for Λ production, with ratios of $R(\Sigma^+/\Sigma^0) = \sigma(pp \to K^+n\Sigma^+)/\sigma(pp \to K^+p\Sigma^0) = 230\pm70$ at $\varepsilon = 13$ MeV and 90 ± 40 at 60 MeV [8]. Such values would imply a very anomalous energy dependence, since bubble chamber data yield a ratio of $R(\Sigma^+/\Sigma^0) = 2.3 \pm 0.9$, though at the much higher excess energy of $\varepsilon = 350$ MeV [9].

In an effort to understand the situation, a first measurement of the $pp \to K^+n\Sigma^+$ reaction was carried out at the COSY-ANKE facility that did not rely on the detection of the final neutron [7]. This experiment at $\varepsilon = 129$ MeV ($T_p = 2.16$ GeV) involved a three pronged approach. Although the statistics were low, apart from a small $K^+n\Lambda\pi^+$ background, the detected $K^+\pi^+$ coincidences at this energy could only have come from $K^+n\Sigma^+$, where the hyperon decays through $\Sigma^+ \to n\pi^+$ (BR = 48.3%). This approach indicated that $R(\Sigma^+/\Sigma^0)$ was of the order of unity at this energy.

Information on the $K^+n\Sigma^+$ channel could also be ob-

*Electronic address: y.valdau@fz-juelich.de

tained through the measurement of K^+-proton correlations, where the Σ^+ shows up as a contribution in the missing-mass distribution via its decay $\Sigma^+ \to p\pi^0$ (BR = 51.6%). Although the overall spectra are sensitive to the model used to describe the dominant $K^+p\Lambda$ channel, at high K^+p missing masses there can only be contributions from Σ production. Both this study and that of the inclusive K^+ production showed consistency with the $K^+\pi^+$ determination and clearly excluded a large value of $R(\Sigma^+/\Sigma^0)$.

These first ANKE results were obtained at a significantly higher excess energy than those of COSY-11 [8] and so did not rule out the possibility of a strong threshold anomaly. The aim of the present work is to extend the earlier ANKE methodology by making four measurements that cover the near-threshold region as well as one below the Σ threshold to obtain data where the $K^+p\Lambda$ channel is the only source of associated strangeness production [10]. The beam energy range covered was from 1.775 to 2.020 GeV.

We start by summarizing in Sec. II the existing near-threshold data on hyperon production in proton-proton collisions and their interpretation in terms of phenomenological models. The ANKE experimental facility used for the study of the $pp \to K^+n\Sigma^+$ reaction and the techniques involved there are described in Sec. III. Section IV presents first the results of the measurements of inclusive K^+ production. The comparison of these data taken just above with those from just below the Σ thresholds allows us to set an upper limit on the Σ^+ production cross section at $\varepsilon = 13$ MeV that is almost two orders of magnitude smaller than the COSY-11 result [8]. The K^+p missing-mass spectra lead to values of the total cross sections for both Λ and Σ^0 production that are in agreement with the world data. The high ends of these spectra can only be populated by events arising from Σ production and these allow first estimates to be made of the Σ^+ cross section as well as conservative upper limits. Although the statistics here are reasonable, it is hard to quantify the systematic uncertainties and, in this respect, the most reliable determination of the Σ^+ production cross section is through the study of $K^+\pi^+$ coincidences which, at the energies of this experiment, can only arise from Σ^+ decay. The values obtained from this study are completely consistent with those found from the K^+p coincidence data and fall below the upper bounds set by the inclusive data.

The results for the total cross sections are discussed in Sec. V, where they are compared to other measurements of Λ and Σ^0 production as well as those of Σ^+. The clean determinations of the $pp \to K^+n\Sigma^+$ cross section from the $K^+\pi^+$ and K^+p measurements give values that are more than two orders of magnitude lower than those reported in the literature through the detection of the neutron [8]. Our conclusions and outlook for the future are presented in Sec. VI.

II. HYPERON PRODUCTION IN PROTON-PROTON COLLISIONS

In the low energy regime (around $T_p \approx 2$ GeV) there are three associated-strangeness production channels allowed in proton-proton collisions, viz. $K^+p\Lambda$, $K^+p\Sigma^0$, and $K^+n\Sigma^+$. Measurements of inclusive K^+ spectra lead to distributions where there are contributions from all three final states. There is no possibility of distinguishing between the different reaction channels without modeling the distributions from all of them [11, 12], and this can lead to severe ambiguities. The basic problem here is that the cross section for Λ production well away from threshold is much larger than those for the Σ close to threshold and there is no reason to believe that the associated distributions should vary like phase space.

The conditions improve when two particles are detected in the final state. Signals from the $pp \to K^+p\Lambda$ and $pp \to K^+p\Sigma^0$ reactions are usually identified through the corresponding peaks in the K^+p missing-mass spectra [3]. The physical backgrounds in such measurements are mostly connected with the decays of Λ and Σ^0 hyperons, which lead to a second proton in the final state (see Table I). The remaining part of K^+p missing-mass spectra can be associated with the $pp \to K^+n\Sigma^+$ reaction channel, where the $\Sigma^+ \to p\pi^0$ decay gives rise to the proton that is detected. It is important to note that the missing-mass range that is obtained using a proton from Λ decay does not extend as far as that linked to Σ production so that the study of the maximum missing-mass region allows one to derive values for the weighted sum of Σ^0 and Σ^+ production. Nevertheless, the contributions are rather small and systematic effects can be significant near this kinematic limit.

However, below the threshold for $pp \to K^+n\Lambda\pi^0$ production ($T_p = 1.975$ GeV), the only source of the $K^+\pi^+$ correlations is Σ^+ production and this provides a much more reliable way to identify the channel than the alternative of detecting the neutron [8]. Although the measurement of $K^+\pi^+$ coincidences provides a very clean signal for the identification of the $pp \to K^+n\Sigma^+$ reaction, the statistics achievable at ANKE are quite low [7, 10].

Final state	$K^+p\Lambda$	$K^+p\Sigma^0$	$K^+n\Sigma^+$
$T_{\rm thr}$ [GeV]	1.582	1.794	1.789
BR(K^+p) [%]	63.9	63.9	51.6
BR($K^+\pi^+$) [%]	–	–	48.3

TABLE I: Characteristics of the three hyperon production channels in proton-proton collisions studied in this experiment. In addition to the threshold beam energies, also shown are the fractions of the cross sections (BR) associated with the $K^+\pi^+$ and indirect K^+p coincidences.

It is evident from the inclusive K^+ production data that there is a strong Λp final state interaction at low invariant masses [11, 13]. This is reflected in the energy dependence of the $pp \to K^+p\Lambda$ total cross section

analyzed in Refs. [12, 14], where the near-threshold experimental data are enhanced compared to phase space. Significant influence of the Λp final state interaction has also been found in the analysis of $pp \to K^+p\Lambda$ Dalitz plots [4, 6]. The measured distributions have been described using a Λ production model which, in addition to the strong FSI, includes the $N^*(1650)$-isobar in the production mechanism. It is believed that this is the dominant resonance in the ≈ 2 GeV region [4].

The ANKE acceptance for the $pp \to K^+p\Lambda$ reaction changes significantly over the energy range where the data were collected. In addition, different models have been used in this analysis for the estimation of the Λ total cross section at different energies. A three-body phase space, modified by the Λp FSI, has been used for $T_p < 1.9$ GeV. Above 1.9 GeV, a model for the $pp \to K^+p\Lambda$ reaction, similar to the one used for the 2.16 GeV data [7], has been developed. This assumes the dominance of the $N^*(1650)$-resonance in the production mechanism and a strong Λp final state interaction. In addition to these effects, there is some anisotropy in the angular spectra of the kaon and direct proton in the $K^+p\Lambda$ final state [15–18]. Unfortunately, unlike the case for the 2.16 GeV data [18], there are no measurements of the angular distributions directly at the energies of interest. The relevant parameters have therefore been determined from linear interpolation of the results of Refs. [15–18] at nearby energies. More details of the model and the parameters used in the Monte Carlo simulations can be found in Ref. [10].

Extensive measurements of the total cross section for Σ^0 production close to threshold were carried out by the COSY-11 collaboration [3, 5]. Some studies of differential observables were undertaken at the COSY-TOF facility [2], though most of the results have only been reported in theses [17, 18]. There is little evidence from these data that in the vicinity of threshold there are significant deviations from phase space. We therefore use a phase-space description when evaluating the acceptance for Σ^0 production at ANKE. Since there is no experimental information at all on differential quantities for the $pp \to K^+n\Sigma^+$ reaction channel at low energies, a similar three-body phase-space description has been employed for Σ^+ production.

The $pp \to K^0p\Sigma^+$ reaction was studied at $\varepsilon = 126$ [19] and 161 MeV [20] during the COSY-TOF pentaquark searches. The value of the total cross section deduced from these data at the lower energy is quite close to that found for the $K^+p\Sigma^0$ final state [18] and this already allows simple bounds to be placed on the cross section for the $pp \to K^+n\Sigma^+$ reaction.

There are only two independent isospin amplitudes for Σ production in proton-proton collisions and these can be taken to correspond to the $I = 1/2$ and $I = 3/2$ combinations of the final ΣN pair. There is therefore a linear relation between the amplitudes for the production of the three possible final states:

$$f(pp \to K^+n\Sigma^+) + f(pp \to K^0p\Sigma^+) + \sqrt{2}\, f(pp \to K^+p\Sigma^0) = 0\,. \quad (1)$$

This leads to a triangle inequality between the total cross sections [9], which can provide model-independent limits on the ratio of Σ^+ to Σ^0 production:

$$\left[\sqrt{\sigma(pp \to K^0p\Sigma^+)} - \sqrt{2\sigma(pp \to K^+p\Sigma^0)}\right]^2 \le \sigma(pp \to K^+n\Sigma^+) \le \left[\sqrt{\sigma(pp \to K^0p\Sigma^+)} + \sqrt{2\sigma(pp \to K^+p\Sigma^0)}\right]^2 . \quad (2)$$

The COSY-TOF result at $\varepsilon = 126$ MeV [19] suggests that at the energy of the earlier ANKE experiment at 2.16 GeV the ratio $R(\Sigma^+/\Sigma^0)$ of the total cross sections for Σ^+ to Σ^0 production should lie in the range $1/6 < R(\Sigma^+/\Sigma^0) < 6$. Though weak, this bound is an order of magnitude smaller than that found by the COSY-11 collaboration, though at lower energies [8]. A direct measurement of the $pp \to K^+n\Sigma^+$ cross section at this energy using the COSY-TOF spectrometer [21] satisfies well this inequality, whereas an earlier one at $\varepsilon = 94$ MeV seems to be much too large [22].

III. EXPERIMENT

The experiment was carried out at the ANKE facility [23] with an unpolarized proton beam provided by the Cooler Synchrotron and storage ring COSY [24]. Of the five beam energies used, $T_p = 1.775$, 1.826, 1.920, 1.958 and 2.020 GeV, the first, just below the threshold for the production of the Σ hyperon, was used for background studies. The values of the excess energies ε for the three final states are given in Table II.

Final state		$K^+p\Lambda$	$K^+p\Sigma^0$	$K^+n\Sigma^+$
p GeV/c	T_p GeV	ε MeV		
2.546	1.775	70	–	–
2.600	1.826	88	11	13
2.700	1.920	122	45	47
2.740	1.958	135	58	60
2.806	2.020	157	80	82

TABLE II: Values of the excess energies ε for the three reaction channels at the five beam momenta p and energies T_p used in this experiment.

The ANKE magnetic spectrometer, located at an internal target position of COSY, is composed of three dipole magnets. $D1$ and $D3$ bend the direct proton beam from the undisturbed COSY orbit to the ANKE target and return it back, respectively. The analyzing magnet $D2$, placed between $D1$ and $D3$, was operated in this experiment with a field strength of $B = 1.57$ T. This magnet

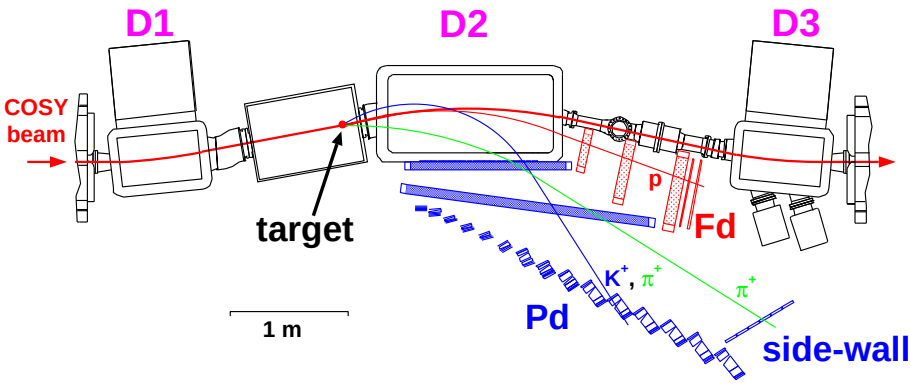

FIG. 1: (Color online) Sketch of the relevant parts of the ANKE detector system showing the positions of the two bending magnets $D1$ and $D3$ and the target before the analyzing magnet $D2$. Only information from the forward (Fd) and positive side (Pd) detectors, including the stop counters in the side wall, was used in this experiment.

deflects positively charged particles with laboratory polar angles up to 20° towards the positive side (Pd) and forward (Fd) detector systems. The high density of the unpolarized H_2 cluster-jet target [25] gave a typical target thickness of $\sim 10^{14}$ atoms/cm^2 and this resulted in an average luminosity of the order of ~ 2 nb^{-1}s^{-1}. In the present analysis only the positive side (for the π^+, K^+ and p identification) and forward detector systems (for proton identification) have been used. A sketch of the ANKE detector system is presented in Fig. 1.

The positive side detector system consists of 23 start (Sa) and 21 stop (So) counters for time-of-flight (TOF) measurements and two multiwire proportional chambers (MWPC) for track reconstruction and background suppression. Depending on the type and momentum of the particle, the tracking efficiencies of the Pd MWPCs are typically $\sim 90\%$, the values being determined using experimental data. The momentum resolution in the positive side detector system is about 2% (FWHM).

The first fifteen stop counters are part of the range telescope system designed for the identification of low momentum K^+ ($p_K^{\rm max} \approx 620$ MeV/c for $B = 1.57$ T) [26]. The remaining six stop counters, joined together to form the side-wall detector ($p^{\rm max} \approx 920$ MeV/c for $B = 1.57$ T), were used for π^+ and p identification on the basis of time-of-flight criteria.

Each of the range telescopes is made up of a stop counter, an energy loss counter (ΔE), a so-called delayed veto counter, and two passive degraders made of copper. The thickness of the first degrader is chosen such that a K^+ deposits all its energy in the ΔE counter and stops either at the edge of it or in the second degrader. The products from the K^+ decay are registered in the delayed veto counter with the characteristic decay time of 12.4 ns. All the range telescopes, placed in the focal plane of the $D2$ magnet, are optimized for the measurement of a given K^+ momentum. The delayed veto criteria leads to a suppression of better than 10^{-5} in the non-kaon background for both inclusive and coincidence measurements. The details of the K^+ identification using the delayed veto technique can be found in Ref. [26].

Due to the unchanged $D2$ magnetic field, the geometry of the positive side detector system was fixed with respect to $D2$ so that the acceptance of each telescope remained the same at all the beam energies where experimental data were collected. As a consequence, the same set of detector efficiencies and acceptances could be used in the analysis of the inclusive data collected at different energies.

The ANKE forward detector system used for the K^+p correlation measurements and the luminosity determination consists of two multiwire proportional chambers, one drift chamber, and a hodoscope of scintillator counters [27]. The tracking efficiency of the Fd chambers, as determined from the experimental data, is homogeneous over the Fd acceptance and is better than 95% for protons. The ensemble of chambers used in the experiment allows the reconstruction of the proton momentum with a precision of $\sim 2\%$ (FWHM). The Fd hodoscope comprises two layers of plastic scintillator counters shifted with respect to each other by half the width of a counter. The two-layer structure allows the time from individual counters to be calibrated with respect to each other by using tracks of particles which cross counters that overlap in different layers. The time signals from individual forward counters are therefore aligned such that in the analysis the full hodoscope can be treated as a single counter [27].

In order to normalize the experimental data, and hence extract absolute cross sections for Σ^+ production, the proton-proton elastic scattering rate was measured using the Fd detector. Due to the high count rate from this reaction channel, a dedicated trigger, prescaled by a factor of a thousand, was used. Having determined the momentum of a proton candidate in the Fd, the $pp \to pp$ reaction was identified via the missing-mass technique. The elastic scattering peak, with a width of 50 MeV/c^2 (FWHM), is well separated from the inelastic background

arising from pion production. The numbers of protons scattered between laboratory angles of 6° and 9° were determined from a fit to the data by a Gaussian with polynomial background. Predictions for the *pp* elastic differential cross section from the SAID analysis [35] were then used to evaluate the luminosity. For all the beam energies in the experiment, the shape of the differential cross section as a function of laboratory angle agreed with the predictions to better than 3%. The luminosity was determined with an overall uncertainty of 7%. This takes into account a 5% estimate of the uncertainty from the SAID program, 3% uncertainty in the analysis algorithm, and 3% uncertainty in the Fd MWPC efficiency determination. The values of the total luminosities accumulated are reported in Table IV.

The Runge-Kutta method of momentum reconstruction was employed for the final analysis. This uses all the information from the chambers and the measured $D2$ magnet field map [28]. The precise knowledge of the particle trajectories provided by this method allows one to calibrate absolutely the times between different start-stop counters in the Pd using experimental data with a π^+ or any other cleanly selected particle. The internal delays for time signals do not change during the experiment and the required constants could be calculated using time information from individual counters and corresponding tracks. After performing the time calibration, the invariant mass of a particle with a given track could be calculated.

The time-of-flight spectra measured at 1.920 GeV for K^+ selected using the delayed veto technique are presented in Fig. 2 summed over all stop counters.

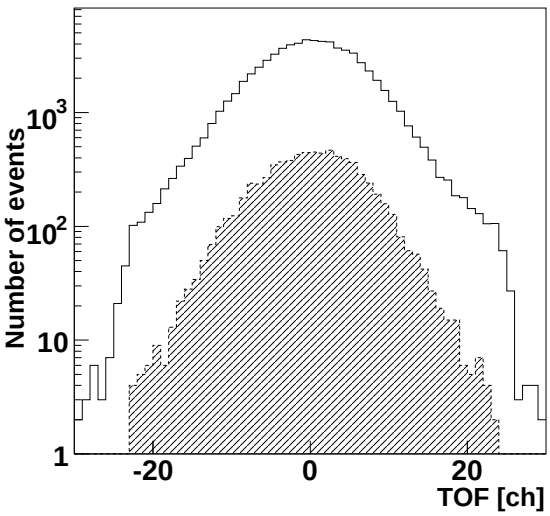

FIG. 2: Time-of-flight (TOF) spectra, measured at 1.920 GeV with a delayed veto, presented on a logarithmic scale. The data, measured in units of 44 ps per channel, have been centered around zero. The hatched histogram shows the distributions of K^+ events for which there were K^+p coincidences.

For the extraction of the inclusive double-differential cross section, the residual background was subtracted from the time-of-flight spectra measured in individual stop counters. The number of K^+ detected in an individual telescope, N_{K^+}, has been determined using a fit of the TOF spectra that assumes a Gaussian peak from the kaons and a flat background. The background contribution to the individual stop counter distributions is less than 5%.

The laboratory cross section has been evaluated for every momentum bin from

$$\frac{d^2\sigma_{K^+}}{d\Omega\, dp}(T_p) = \frac{N_{K^+}}{\Delta p\, \Delta\Omega} \frac{1}{L_{\rm tot}\, \epsilon_{K^+}}, \qquad (3)$$

where $\Delta\Omega$ is the solid angle integration region and $L_{\rm tot}$ the integrated luminosity. A momentum bin of $\Delta p = 24$ MeV/c was imposed in the course of the data analysis. The efficiency of K^+ identification, ϵ_{K^+}, is estimated on the basis of

$$\epsilon_{K^+} = \epsilon^{\rm tel} \times \epsilon^{\rm scint} \times \epsilon^{\rm MWPC} \times \epsilon^{\rm acc}\,. \qquad (4)$$

Due mainly to geometric acceptance factors, the delayed-veto technique leads to a telescope efficiency $\epsilon^{\rm tel}$ of about 30% for low momentum kaons but only 10% for the highest momenta [26]. The value for each telescope has been determined with a precision of 5% by using K^+p correlations recorded with a dedicated trigger. The scintillator counter efficiency $\epsilon^{\rm scint}$ is higher than 98% while that of the MWPC, $\epsilon^{\rm MWPC}$, varies between $90-95$%, depending on the K^+ momentum. These efficiencies have been determined using experimental data. The acceptance correction factor $\epsilon^{\rm acc}$ has been estimated using a GEANT4 [29] model of the ANKE spectrometer. The overall K^+ detection efficiency ϵ_{K^+} in this measurement is independent of beam energy.

The K^+p missing-mass spectra, which depend on the data measured with the Fd detector, have been used to extract cross sections for the Λ and Σ^0 production channels. For the selection of K^+p pairs detected in the forward and positive detectors, the time differences between the K^+ in the Pd and the proton in the Fd have been calculated. A 3σ cut has been applied to subtract the residual background from accidental coincidences. The background in the K^+p coincidence spectra measured with the delayed veto is less than 2%.

The K^+ time-of-flight spectrum measured in coincidence with the proton detected in the Fd at 1.920 GeV is shown in Fig. 2 by the hatched histogram. The overall reduction between the K^+ TOF spectra measured with and without the proton being detected in the Fd is due to the acceptance of this detector. The numbers of Λ and Σ^0 events, $N_{\rm ev}$, in the spectra were estimated using fits of the simulations to the K^+p missing-mass spectra. The

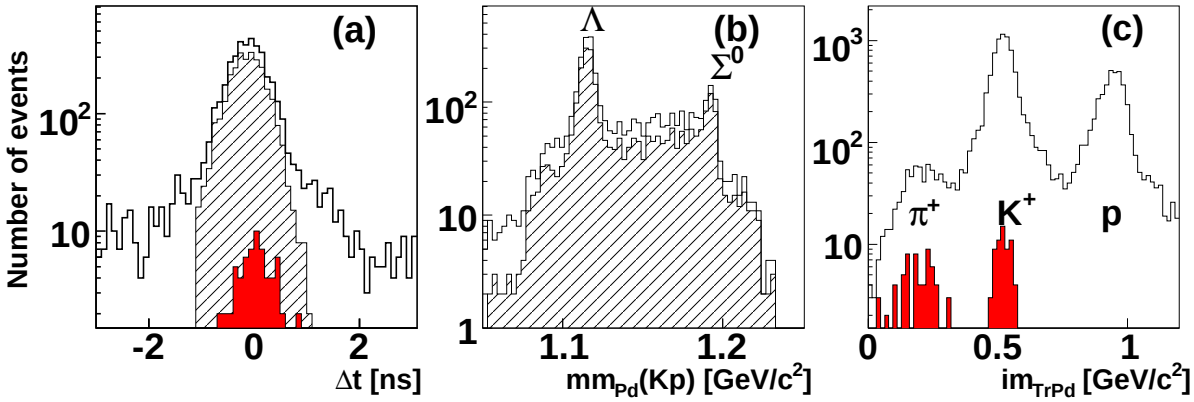

FIG. 3: (Color online) Identification of two-particle events in the positive side detector at 1.920 GeV, where a cut of $\theta_{K^+} < 12^\circ$ has been imposed on the K^+ angle. (a) The difference Δt between measured and calculated times of the correlated particles. The selection of double coincidences in Pd is shown by the hatched histogram for K^+p and the filled histogram (red) for $K^+\pi^+$ pairs. (b) The K^+p missing-mass spectra measured in Pd. The hatched histogram represents K^+p missing mass selected using the cuts shown in panel (a). (c) The invariant mass of a detected particle before and after (filled histogram) the selection of $K^+\pi^+$ coincidences using the criteria in panel (a).

total cross sections were then evaluated from

$$\sigma_{\rm total} = \frac{N_{\rm ev}}{L_{\rm total}\,\epsilon^{\rm sum}}\,, \qquad (5)$$

where $L_{\rm tot}$ is the integrated luminosity, $\epsilon^{\rm sum}$ the overall efficiency that includes the detector efficiencies, the in-flight K^+ decay correction, and the total acceptance within a particular reaction model, as discussed in Sec. II.

The rate of $K^+\pi^+$ coincidences is very small. Therefore, the K^+p correlations detected in the positive detector have been used to optimize the cut parameters and selection criteria. The K^+ and p tracks were selected using time-of-flight criteria. In Fig. 3a the difference between calculated and measured time in the So counters is shown, with its center shifted to zero. Also presented in panels b and c are the distributions in missing mass, assuming that tracks are from K^+p coincidences, and the invariant mass of the particles whose tracks are detected in the Pd. The hatched histogram in Fig. 3b represents K^+p coincidences selected using a 3σ cut on the time difference shown in panel a. The number of Λ and Σ^0 events, estimated using the clear peaks in the missing-mass distribution, hardly change. This indicates that the efficiency of the cuts is better then ~ 97 %.

When the same cuts on the time difference are applied to the $K^+\pi^+$ candidates, the results found are shown in Figs. 3b and c by filled histograms. Since it is impossible to get correct time information for events where both particles are detected in the same counter, these are dropped from the analysis. This effect is most serious for the $K^+\pi^+$ coincidences at lowest energy but even there it does not exceed 25%. An additional correction factor has been introduced to compensate for the loss.

The number of $K^+\pi^+$ correlated pairs has been used to evaluate the total cross section for Σ^+ production on the basis of Eq. (5). This includes a correction for the corresponding branching ratio (48.3%) reported in Table I. The acceptance calculation, as well as the reaction models used, are discussed in Sec. II and given in more detail in Ref. [10].

IV. EXPERIMENTAL RESULTS

A. Inclusive counting rates

A first limit on the cross section for Σ^+ production can be obtained by comparing the inclusive K^+ counting rates just above the Σ thresholds with those just below. Figure 4 shows the ratio of the data obtained at 1.826 GeV to those at 1.775 GeV as a function of the kaon laboratory momentum. In this way any questions regarding telescope efficiencies and acceptances are avoided. At 1.826 GeV the K^+ mesons associated with Σ^+ production have a maximum laboratory angle of $\vartheta_{K^+}^{\rm max} = 12.2^\circ$ and a momentum range from 352 to 643 MeV/c. Essentially the whole phase space for Σ production is therefore sampled in the data, though the vertical angular limitation and, to some extent, the horizontal angle cut of 12° and the ± 12 MeV/c momentum cut for each telescope reduces the acceptance to about 23%. The simulations discussed in Sec. II suggest that the contribution to the ratio from Λ production should be essentially constant over the whole momentum range, independent of any assumptions made regarding the kaon angular distributions.

The ratio of differential cross sections can be expressed by Eq. (6):

$$R\left(\frac{1.826}{1.775}\right) = \frac{\Lambda_{1.826}}{\Lambda_{1.775}} + \frac{\Sigma^0_{1.826} + \Sigma^+_{1.826}}{\Lambda_{1.775}} \qquad (6)$$

The shape expected for the contribution from the combined $pp \to K^+p\Sigma^0$ and $pp \to K^+n\Sigma^+$ channels is indicated, using total cross sections $\sigma(\Sigma^0) = \sigma(\Sigma^+) = 0.021$ μb, $\sigma_{1.826}(\Lambda) = 7.9$ μb and $\sigma_{1.775}(\Lambda) = 6.1$ μb. Depending upon how the Λ level is drawn, this comparison gives a cross section ratio of $(\sigma(pp \to K^+p\Sigma^0) + \sigma(pp \to K^+n\Sigma^+))/\sigma(pp \to K^+p\Lambda) = (4 \pm 2) \times 10^{-3}$, from which we deduce that the total cross section for Σ^+ production at 1.826 GeV ($\varepsilon = 13$ MeV) is below 45 nb at the 98% confidence level. This upper bound already excludes the COSY-11 result [8] by a very large margin. Even if the ratio of the Σ^+/Σ^0 production cross sections were a factor of six, as allowed by the triangle inequality at $\varepsilon = 129$ MeV, the resulting distribution would greatly overestimate the data shown in Fig. 4.

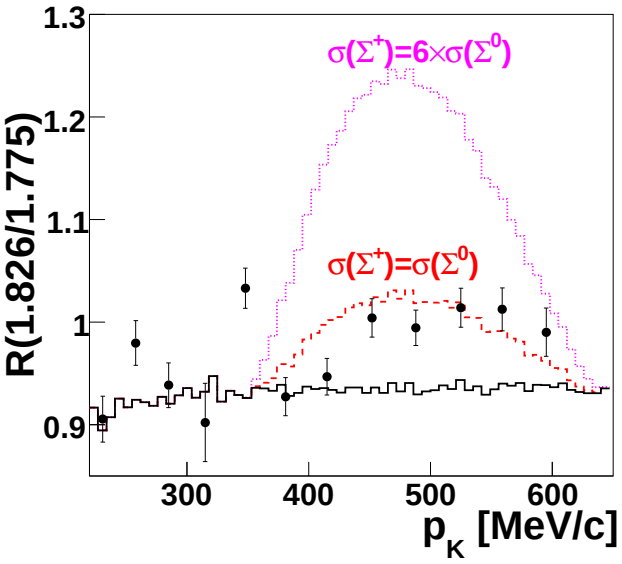

FIG. 4: (Color online) Ratio of normalized count rates for inclusive K^+ production at 1.826 GeV to those at 1.775 GeV as a function of the momenta in the different telescopes. The data were taken using the ANKE range telescope system with $\vartheta_{K^+} < 12°$ and a 12 MeV/c momentum cut for each telescope. The black solid histogram represents the simulation for the $pp \to K^+p\Lambda$ reaction, whereas the dashed red one includes also contributions from Σ^+ and Σ^0 production, assuming $\sigma(\Sigma^0) = \sigma(\Sigma^+) = 0.021$ μb, $\sigma_{1.826}(\Lambda) = 7.9$ μb and $\sigma_{1.775}(\Lambda) = 6.1$ μb. The upper magenta dotted histogram represents a simulation where the Σ^+ total cross section is taken to be six times that of Σ^0, which is the limit allowed by the triangle inequality at $\varepsilon = 129$ MeV.

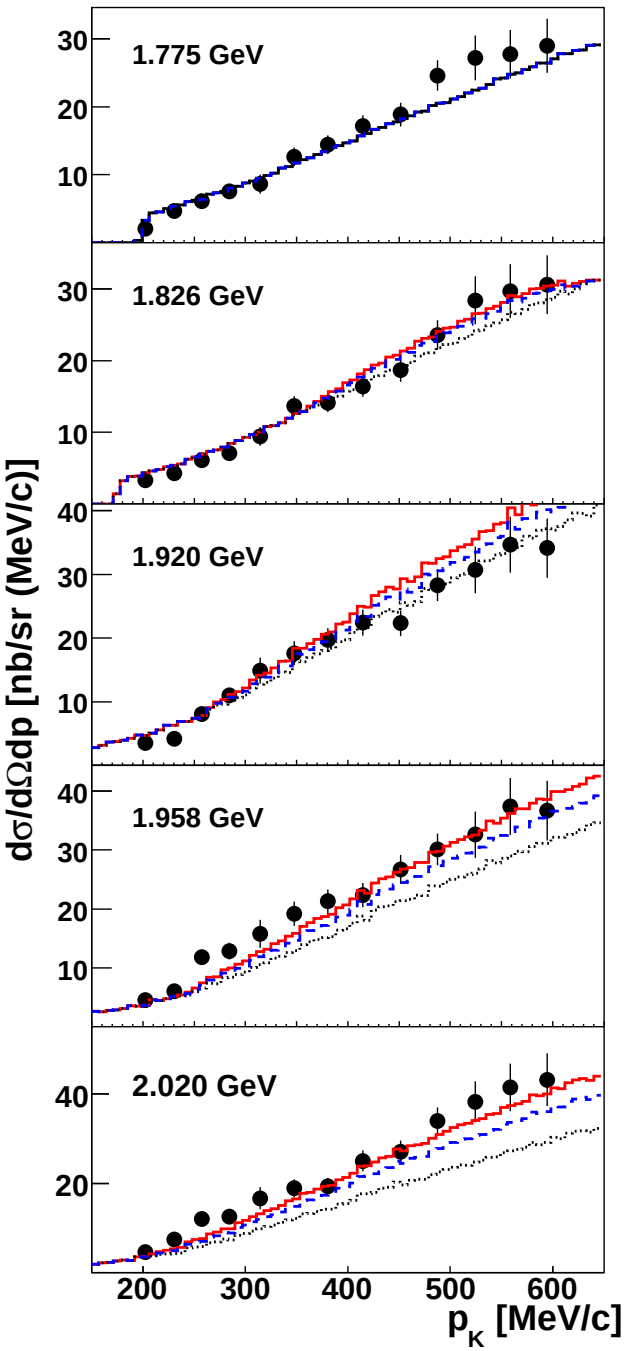

FIG. 5: (Color online) Laboratory differential cross sections for inclusive K^+ production at the five measured energies, evaluated over the angular region $\vartheta_K < 4°$. The overall uncertainty of 7% coming from the luminosity has not been included. The experimental results are compared with Monte Carlo simulations; Λ production (black dotted line), $\Lambda + \Sigma^0$ production (blue dashed line), $\Lambda + \Sigma^0 + \Sigma^+$ production (red solid line).

B. Inclusive cross sections

The average momentum p_K of the K^+ meson, detected in each of the telescopes, as well as the corresponding values of the inclusive double-differential cross sections, evaluated using Eq. (3), are presented in Table III. These have then been summed and averaged over the kaon an-

gular range $\vartheta_{K^+}<4^\circ$ to give the inclusive cross sections shown in Fig. 5 for the five beam energies studied. The data are compared with simulations of Λ, Σ^0 and Σ^+ production discussed in Sec. II, where the individual contributions from the three reaction channels have been normalized to the total cross sections deduced from the K^+p and $K^+\pi^+$ correlation data, as described in Sec. V. Although there is fair agreement between the simulations and the data for all five energies, it has to be stressed there is considerable ambiguity in the dominant Λ production cross section because in this case the reaction is measured far above threshold. The COSY-TOF results show that there are then strong deviations from phase space for both the angle and momentum of the K^+ [6].

C. Kaon-proton coincidence measurements

The K^+p missing-mass spectra measured at four beam energies are presented in Fig. 6. Due to technical problems in the preparation of the K^+p correlation trigger, the spectrum measured at 1.826 GeV could not be reconstructed reliably and is therefore not shown. However, this problem does not affect either the K^+ inclusive or the $K^+\pi^+$ correlation data collected at this energy.

Figure 6 shows clear peaks associated with the $pp \to K^+p\Lambda$ and $pp \to K^+p\Sigma^0$ production processes, where the "p" corresponds to the proton that is detected in ANKE. For events that lie within the Σ^0 peak, the distributions of K^+ missing masses are consistent with predictions based upon a phase-space production model, with no evidence for any strong $\Sigma^0 p$ final state interaction.

In addition to the direct protons, there are large "indirect" physics backgrounds, where the K^+ is measured in coincidence with a proton that arises from the decay of one of the hyperons produced. The values of the relevant decay fractions are given in Table I. Both types of contribution from the three reaction channels have been simulated and traced through the GEANT4 model of the ANKE spectrometer. In view of their proximity to the thresholds, as well as the evidence discussed above, the contributions to the spectra from the two Σ channels have been estimated using simple phase-space descriptions. However, Λ hyperon production, which dominates the distributions, has been simulated using the different models mentioned in Sec. II. In all cases the protons that were produced in the decay of the three hyperons were assumed to be distributed according to phase space.

The numbers of detected Λ and Σ^0 events could be fixed reliably from fits to the experimental peaks and do not depend significantly on the model used for the Λ production. The indirect protons from Λ decay lead to a missing-mass distribution that dies off well before the kinematic limit, as can be judged from the simulations shown in Fig. 6. Above the Λ limit there are contributions coming from protons from Σ^0 and Σ^+ decay and these give rise to distributions with somewhat different shapes. The numbers of Σ^0 events expected in this region

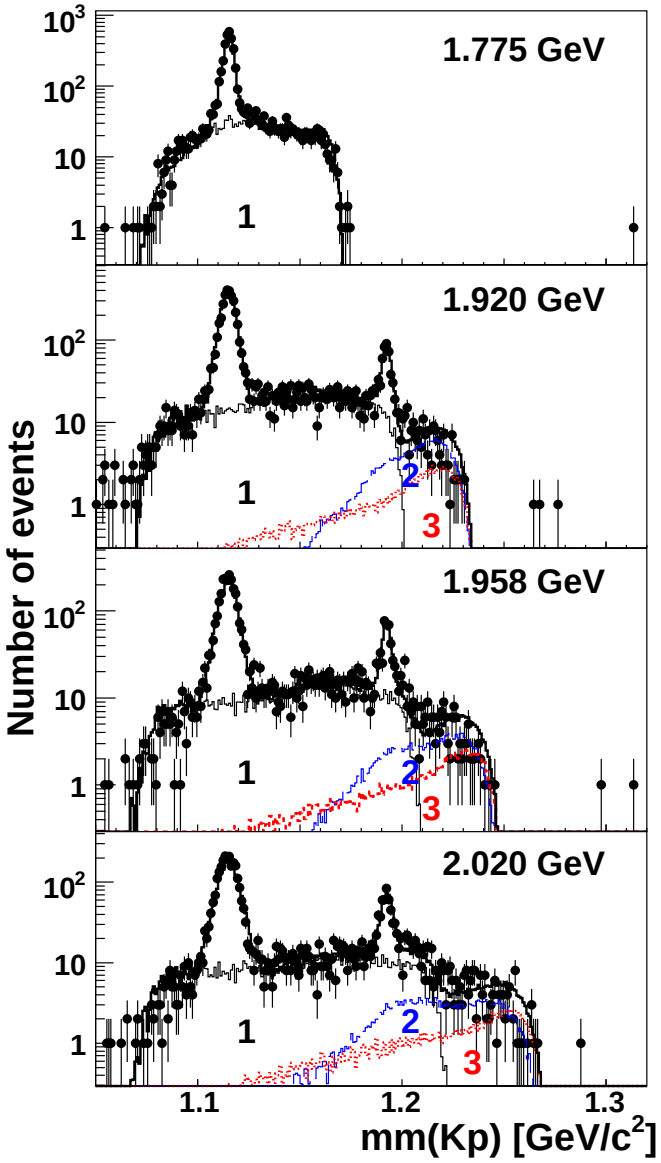

FIG. 6: (Color online) The K^+p missing-mass spectra measured at four beam energies (closed symbols) compared to simulations normalized to the total cross sections listed in Tables V and VI. In addition to the protons from $pp \to K^+p\Lambda/\Sigma^0$, these include contributions from indirect K^+p correlations involving decay protons arising from the production of the Λ (histogram 1), Σ^0 (histogram 2 (blue)), and Σ^+ (histogram 3 (red)). As explained in the text, the K^+p correlation data were unreliable at 1.826 GeV and so results are not shown for this energy.

can be estimated from the population in the Σ^0 peak and, by subtraction, the numbers of Σ^+ events can be estimated. The resulting values for the Σ^+ production cross section are 0.25 ± 0.05, 0.41 ± 0.09, and 1.09 ± 0.16 μb at 1.920, 1.958 and 2.020 GeV, respectively. Only statistical error bars are quoted and it is hard to obtain robust

p_K MeV/c	$d\sigma/d\Omega dp$ nb/(sr MeV/c)					R(1.826/1.775)
231	4.7 ± 0.5	4.3 ± 0.5	4.2 ± 0.5	6.1 ± 0.7	7.5 ± 0.9	0.91 ± 0.02
258	6.1 ± 0.7	6.1 ± 0.7	8.1 ± 0.9	11.8 ± 1.3	12.0 ± 1.3	0.98 ± 0.02
285	7.6 ± 0.9	7.1 ± 0.8	11.0 ± 1.2	12.8 ± 1.4	12.6 ± 1.4	0.94 ± 0.02
315	8.6 ± 1.4	9.4 ± 1.3	14.9 ± 2.1	15.8 ± 2.4	16.7 ± 2.5	0.90 ± 0.04
348	12.6 ± 1.4	13.6 ± 1.4	17.6 ± 1.9	19.2 ± 2.1	18.9 ± 2.0	1.03 ± 0.02
381	14.4 ± 1.4	14.2 ± 1.3	19.7 ± 1.8	21.3 ± 2.0	19.4 ± 1.9	0.93 ± 0.02
415	17.1 ± 1.6	16.4 ± 1.5	22.4 ± 2.0	22.4 ± 2.1	25.0 ± 2.3	0.95 ± 0.02
452	18.9 ± 1.7	18.7 ± 1.7	22.3 ± 2.0	26.7 ± 2.5	27.1 ± 2.5	1.00 ± 0.02
488	24.6 ± 2.2	23.6 ± 2.1	28.3 ± 2.5	30.1 ± 2.7	34.0 ± 3.0	0.99 ± 0.02
525	27.2 ± 3.3	28.4 ± 3.3	30.7 ± 3.7	32.6 ± 3.9	38.3 ± 4.6	1.01 ± 0.02
559	27.8 ± 3.6	29.7 ± 3.7	34.7 ± 4.4	37.4 ± 4.8	41.4 ± 5.3	1.01 ± 0.02
595	29.0 ± 4.0	30.6 ± 4.1	34.2 ± 4.6	36.6 ± 5.1	43.2 ± 5.9	0.99 ± 0.02
T_p [GeV]	1.775	1.826	1.920	1.958	2.020	

TABLE III: The K^+ laboratory double-differential cross sections measured at five beam energies are integrated over $\vartheta_{K^+} < 4^\circ$ and momentum bins of width ± 12 MeV/c. The errors do not include the systematic uncertainty of 7% coming from the normalization. The final column shows the ratio of K^+ count rates measured at 1.826 and 1.775 GeV in the interval $\vartheta_{K^+} < 12^\circ$ and ± 12 MeV/c momentum bins.

estimates of the systematic uncertainties due to the proximity of the kinematic limit. Conservative upper limits on the Σ^+ production cross section can be derived if one assumes that the whole contribution to the spectra above the Λ limit comes from Σ^+ production. This extreme hypothesis gives values of 0.51, 0.83, and 1.62 μb at the three energies. These results are given in Table VI along with those obtained from the $K^+\pi^+$ analysis.

The histograms in Fig. 6 present our estimations for all three reaction channels, normalized to the total cross sections listed in Tables V and VI. If the value of the Σ^+ cross section at 1.958 GeV were as large as that advocated by the COSY-11 collaboration [8], this would require boosting the red histogram in Fig. 6 by about two orders of magnitude.

D. Kaon-pion coincidence measurements

Below the threshold for the $pp \to K^+n\Lambda\pi^+$ reaction ($T_{\rm thr} = 1.975$ GeV), the $K^+\pi^+$ coincidences arising from the hyperon decay $\Sigma^+ \to n\pi^+$ are a unique signature of the $pp \to K^+n\Sigma^+$ reaction. The background from the $K^+n\Lambda\pi^+$ channel will remain negligible also at 2.02 GeV because of the very small phase space and the fact that at the much higher energy of 2.88 GeV it comprises only 4% of the Σ^+ production cross section [9]. The smallness of the $K^+n\Lambda\pi^+$ production rate was also confirmed by our studies at 2.16 GeV, where no evidence for this channel was found in the kaon-proton and kaon-pion coincidence spectra [7].

The measured kaon and pion momentum spectra from $K^+\pi^+$ coincidence events are presented in Fig. 7, where they are compared with phase-space simulations of the $pp \to K^+n\Sigma^+$ reaction. The number of random coincidences that survive the analysis procedure discussed in Sec. III can be judged from the spectra measured at $T_p = 1.775$ GeV, which is below the Σ^+ threshold. The kinematically allowed region in the two dimensional plane of the K^+ and π^+ momenta has been determined from simulations carried out at each energy. The resulting kinematical cuts have been applied, not only on the distributions above threshold, but also on the 1.775 GeV data. To compensate for the random background, the number of events estimated from the subthreshold data has been subtracted from the data at the different energies, taking into account the relative total luminosities.

ε MeV	$L_{\rm tot}$ pb^{-1}	$N_{\rm tot}$ event	$\varepsilon^{\rm acc}_{K^+\pi^+}$ %
13	3.53	16	2.3
47	2.17	54	0.6
60	1.49	54	0.5
82	1.40	69	0.1

TABLE IV: Input information for the Σ^+ total cross section estimation on the basis of the $K^+\pi^+$ correlation data. Values are given for the excess energy (ε), total luminosity ($L_{\rm tot}$), accumulated number of $K^+\pi^+$ coincidences after background subtraction ($N_{\rm tot}$), and total geometrical acceptance used ($\varepsilon^{\rm acc}_{K^+\pi^+}$).

After subtracting the background bin-by-bin and correcting for efficiencies, the K^+ and π^+ momentum spectra measured above the Σ threshold are compared in Fig. 7 with phase-space simulations. Although the numbers of events are small and the fluctuations large, both the K^+ and π^+ distributions are in reasonable agreement with the simulations, within the uncertainties of the background subtraction procedure. The number of $K^+\pi^+$ coincidences extracted from the spectra, together with estimates of the overall geometrical acceptance (see Tab. IV), including all the efficiencies, lead to evaluations of the total cross sections on the basis of Eq. (5).

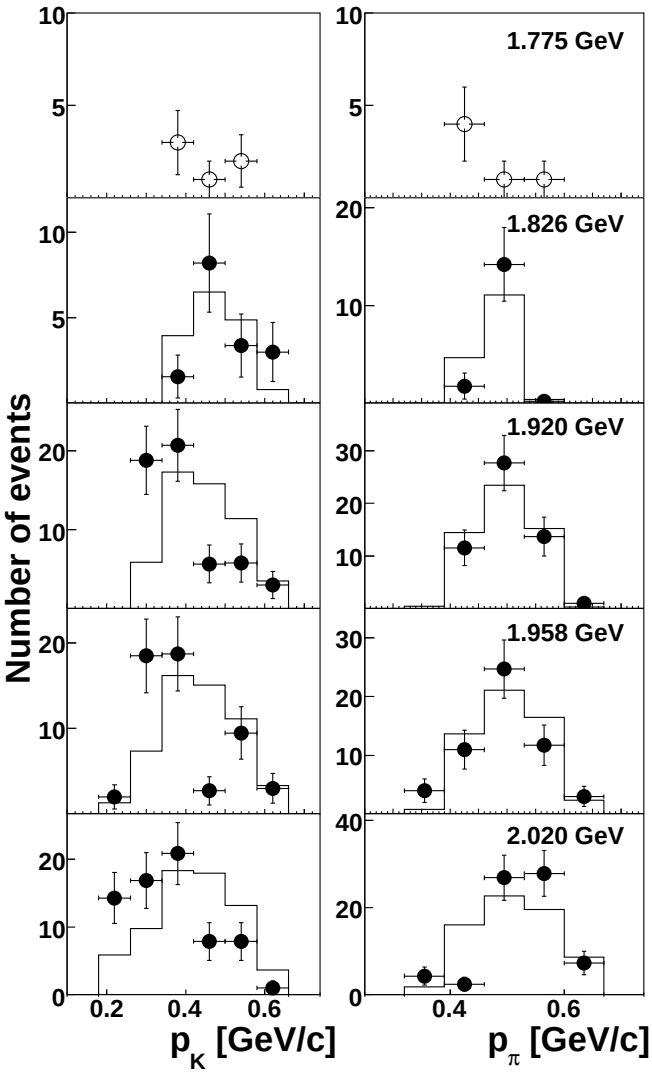

FIG. 7: Spectra of the kaon and pion momenta from identified $K^+\pi^+$ pairs measured at four energies above the Σ^+ threshold and one below. The pions are taken over the full horizontal acceptance of ANKE ($\approx 15^\circ$) whereas the kaons are cut at 12°. Random background has been subtracted bin-by-bin from the above-threshold data by scaling the 1.775 GeV results by the relative luminosity. The spectra are compared to phase-space simulations of the $pp \to K^+n\Sigma^+$ reaction channel.

These are presented in Table VI, where the very satisfactory agreement with the results derived from the K^+p correlation data is demonstrated.

V. TOTAL CROSS SECTIONS FOR HYPERON PRODUCTION

The results obtained for the total cross sections of hyperon production in proton-proton collisions are presented in Table V and VI. The values in the Λ and Σ^0 cases are extracted from the fits to the two peaks in the K^+p correlation spectra of Fig. 6. Since the data were taken far from the Λ threshold where the ANKE acceptance is low, the uncertainties here are dominated by the ambiguities in the models used to describe the differential distributions. Any model dependence is far weaker for Σ^0 production and the contributions from other systematic effects, including luminosity, are of a similar size.

Hyperon	T_p GeV	ε MeV	σ μb	$\Delta_{\rm stat}$ %	$\Delta_{\rm syst}$ %
Λ	1.775	70 ± 1	6.1	2	18
	1.920	122 ± 1	16.9	2	21
	1.958	135 ± 1	16.1	2	21
	2.020	157 ± 1	18.0	2	31
Σ^0	1.920	45 ± 1	0.24	5	14
	1.958	58 ± 1	0.51	5	14
	2.020	80 ± 1	1.30	5	14

TABLE V: Total cross sections for Λ and Σ^0 production measured in proton-proton collisions.

T_p GeV	ε MeV	$\sigma_{K\pi}$ μb	$\Delta_{\rm stat}$ %	$\Delta_{\rm syst}$ %	σ_{Kp} μb	$\Delta_{\rm stat}$ %	Upper limit μb
1.826	13 ± 1	0.011	38	17	–	–	0.045
1.920	47 ± 1	0.20	16	17	0.25	21	0.51
1.958	60 ± 1	0.39	15	17	0.41	23	0.83
2.020	82 ± 1	0.76	14	17	1.09	15	1.62

TABLE VI: Total cross sections for $pp \to K^+n\Sigma^+$ production measured in this experiment. The values in the column marked $\sigma_{K\pi}$ were obtained from the study of the $K^+\pi^+$ coincidence data whereas those in column σ_{Kp} followed from the study of the high K^+p missing-mass spectra of Fig. 6. As discussed in the text, it is very hard to quantify satisfactorily the systematic uncertainties in this case. The upper limit quoted in the last column at 1.826 GeV was derived from the study of inclusive K^+ production above and below threshold shown in Fig. 4. At the higher energies, the upper limits were obtained by assuming that all the events in Fig. 6 that fell above the kinematic limit for the Λ were associated with Σ^+ production.

Table VI shows the values of the Σ^+ production cross section extracted from both the $K^+\pi^+$ and K^+p correlation data shown in Figs. 7 and 6, respectively. As previously remarked, experimental difficulties at $T_p = 1.826$ GeV made the K^+p correlation data unreliable at this energy, though this had no influence on the $K^+\pi^+$ measurement. The principal errors in the $K^+\pi^+$ case arise mainly from the low statistics. These are much better in the K^+p coincidence measurement but the difficulties associated with evaluating the acceptance at the kinematic limit makes it hard to quantify the systematic errors. Despite these uncertainties, the agreement between the two sets of measurements is very reassuring. Upper limits on the Σ^+ production cross section are also quoted in Table VI. That at the lowest energy was extracted at the 98% confidence level from the compar-

ison of the inclusive K^+ production data at 1.826 and 1.775 GeV shown in Fig. 4. At the three higher energies the upper bounds were determined from the assumption that all the events above the Λ limit in the K^+p missing-mass spectra of Fig. 6 corresponded to Σ^+ production. At 1.958 GeV this is about a factor of 50 below the result of the COSY-11 collaboration [8]. It can be seen from the tables that the Σ^+ production cross sections are only a little less than those of Σ^0 but that the difference is within the error bars.

The results for all three hyperons are presented in graphical form in Fig. 8. It is seen from this that our values of the production cross sections for both Λ and Σ^0 are consistent with the world data. However, it has to be stressed once again that a large systematic error bar had to be ascribed to the Λ value because of the small ANKE acceptance. As is well known, it is important to introduce the Λp final state interaction to describe the energy dependence of the $pp \to K^+p\Lambda$ total cross section. On the other hand it is seen that the $pp \to K^+p\Sigma^0$ variation is much closer to phase space, though our data might give a possible hint of some small repulsive FSI.

The Σ^+ production cross section in pp collisions shows no sign of any threshold enhancement of a type that could explain the large values found by the COSY-11 collaboration [8] and, indeed, their values are already completely excluded by the upper bounds provided by the K^+ inclusive and K^+p correlation data of Figs. 4, 5 and 6. The theoretical models [32, 33] whose predictions are shown in Fig. 8b were motivated by the COSY-11 data and fail completely to reproduce our results.

The ratio of Σ^+ to Σ^0 production seems to lie between about a half and one, though the difference is possibly within the error bars. The energy dependence shown in Fig. 8b seems a little steeper than that suggested on phase-space grounds and, if this is so, it could be an indication for a damping effect near threshold due to a Σ^+n final state interaction. There is ample evidence from the study of the threshold cusp in $K^-d \to \pi^-\Lambda p$ [34] that the Λp and ΣN channels are strongly coupled. The enhancement in the K^+ missing mass in the inclusive $pp \to K^+X$ data at the ΣN threshold [11, 13] is a possible sign that flux is being removed from the $pp \to K^+N\Sigma$ channels in this region.

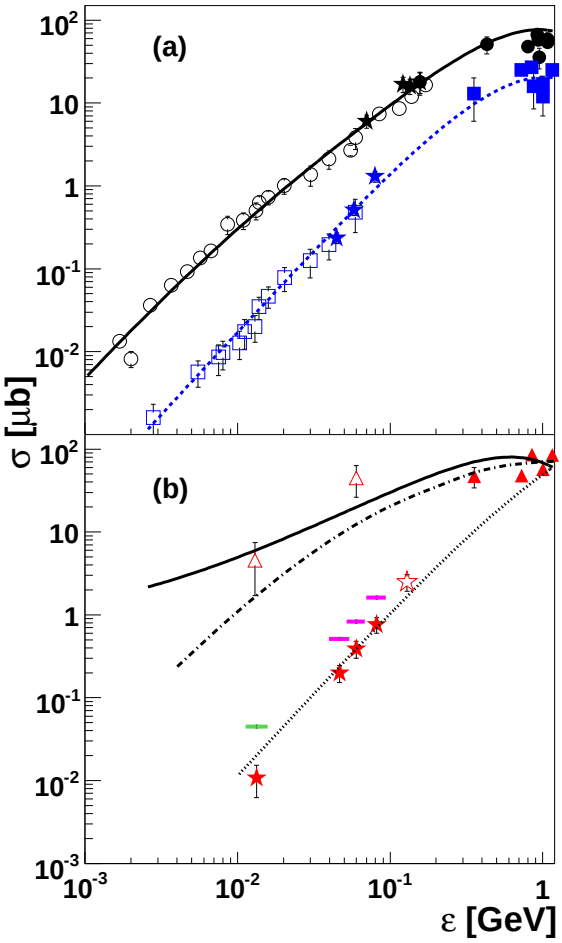

FIG. 8: (Color online) Total cross sections for hyperon production in proton-proton collisions as functions of excess energy obtained in this experiment and compared to published data. Panel (a): Results for Λ (black stars) and Σ^0 (blue stars). The data points obtained in other experiments at COSY and other facilities are shown by open and closed symbols (circles for Λ and squares for Σ^0) [1–3, 5–7, 9, 19, 20, 31]. The lines represent parameterizations of the world data from Ref. [14]. Panel (b): Σ^+ production. Closed stars represent the current data set obtained from the $K^+\pi^+$ coincidence spectra. The open star corresponds to our previous measurement [7]. The conservative upper limits given in Table VI are shown by the four short horizontal lines. The COSY-11 results [8] are shown by open triangles while the closed ones are taken from a compilation of higher energy data [31]. The dotted line corresponds to a pure phase-space variation with a normalization chosen to pass through our central energies. The solid line is a parameterization that includes a strong $n\Sigma^+$ FSI and energy dependent matrix element [32]. The broken line is taken from the microscopic calculation of Ref. [33].

VI. CONCLUSIONS

We have reported measurements of the $pp \to K^+n\Sigma^+$ reaction at four energies close to threshold using two techniques. Instead of identifying the neutron, as was attempted at COSY-11 [8], the K^+ was detected in coincidence with the π^+ that came from the decay of the Σ^+ hyperon. Below the threshold for $K^+n\Lambda\pi^+$ production, this decay is the only source of such correlations. The numbers of random $K^+\pi^+$ coincidences were small and could be estimated from data taken below the threshold for Σ^+ production. These results were confirmed within error bars from the study of the high end of the K^+p missing-mass spectra, though it has to be stressed that systematic effects are harder to control in this measure-

ment. Nevertheless, conservative upper limits on Σ^+ production could be obtained by assuming that the Σ^0 events did not populate the high K^+p missing-mass distributions. In complete contrast to the COSY-11 results [8], we found cross sections for the $pp \to K^+n\Sigma^+$ reaction to be even a little smaller than those of $pp \to K^+p\Sigma^0$.

The large COSY-11 Σ^+ production rates could also be excluded by the study of inclusive K^+ production [12]. However, this does not provide the best estimates of the $pp \to K^+n\Sigma^+$ cross section because the K^+ spectrum is dominated by the $K^+p\Lambda$ channel, unless Σ^+ production is anomalously large near threshold [8]. The uncertainty in the Σ^+ cross section deduced from such data cannot therefore be smaller than the sum of the uncertainties in the models describing Λ and Σ^0 production, which is why these data only provide upper limits on Σ^+ production.

The data on Λ production were taken far above threshold where the acceptance of ANKE for the $pp \to K^+p\Lambda$ reaction is small. The predicted numbers of inclusive K^+ depend sensitively upon the variation of the production with angle and momentum. In addition to the strong distortion due the Λp final state attraction, the COSY-TOF data [6] show significant angular variation. As a consequence, one cannot extract total cross sections for Λ production in a model-independent way from an apparatus with a small acceptance in angle. The situation would be even more uncertain if the strong $\Lambda p \rightleftharpoons \Sigma N$ channel coupling [34] gave rise to a rapid K^+ momentum dependence. Our aim was merely to show that, with reasonable model assumptions, we could achieve total cross sections that were not inconsistent with world data.

The experimental situation regarding acceptance is far more comfortable for the $K^+p\Sigma^0$ channel in this respect because the results were obtained not far above threshold. Furthermore, it is believed that the $\Sigma^0 p$ final state interaction is much weaker than that of the Λp and our data agree with this. The resulting values of the $pp \to K^+p\Sigma^0$ cross section shown in Fig. 8a are completely consistent within error bars with published data and this supports the validity of our experiment and its analysis.

Although the $K^+\pi^+$ coincidence method leads to only small numbers of events within our acceptance, these are very clean and so the total cross sections presented in Fig. 8b have fewer systematic uncertainties than those coming from the K^+p correlation data. It may therefore be interesting to note that, taken together with our 2.16 GeV point [7], the data seem to indicate a somewhat steeper rise than expected on the basis of phase space. This is definitely the case if the data have to join smoothly on to the bubble chamber measurements shown in Fig. 8.

Attractive final state interactions, such as those in the pp or Λp systems, give rise to a very strong energy dependence because they can generate virtual state poles in the production amplitudes. This is not the case when there is repulsion between two final particles and so this would, in general, lead to much smaller effects. There is, however, a third type of final state interaction, namely an absorptive one where the final wave function is damped at small distances rather than being repelled. In the present case this could arise from the coupling of the ΣN and the Λp channels, which is known to be very strong at low energies [34]. It is therefore possible that flux from the $K^+N\Sigma$ channels is lost to feed the $K^+p\Lambda$ channel.

If the coupled channel final state interaction is significant, it would only be relevant in the isospin $I = \frac{1}{2}$ state and this would have twice as big an effect on $K^+n\Sigma^+$ production compared to $K^+p\Sigma^0$. It is perhaps noteworthy that the parameterization of the world data for $pp \to K^+p\Sigma^0$ shown in Fig. 8a do not seem to indicate as steep a rise as for $pp \to K^+n\Sigma^+$, though this is not the case for our own Σ^0 data.

As stressed in Sec. II, there are isospin links between the amplitudes for $pp \to K^+p\Sigma^0$, $pp \to K^+n\Sigma^+$, and $pp \to K^0p\Sigma^+$, but these all refer to an initial NN isospin-one state. The isospin-zero amplitude for $pn \to K^+p\Sigma^-$ is independent of these and so extra help for the modeling might be provided by measurements in this channel. This will be possible at COSY-ANKE through the study of quasi-free production on the deuteron with the detection of the spectator proton [36].

The existing theoretical models for $pp \to K^+n\Sigma^+$ production [32, 33] bear no relation to our results. If the reaction were driven by the exchange of non-strange mesons exciting a Δ isobar [33], this would strongly favor the production of the Σ^+ compared to the Σ^0, which is in conflict with the data. It would also not contribute to the isospin-zero production of Σ^-. Further theoretical work is clearly needed to understand the full data set.

Acknowledgments

We wish to thank the COSY team, especially D. Prasuhn and B. Lorentz for their support throughout this experiment. Useful discussions with A. Sibirtsev and other members of the ANKE Collaboration are gratefully acknowledged. This work has been partially supported by BMBF, Russian Academy of Science, the JCHP FFE, and the HGF-VIQCD.

[1] J.T. Balewski *et al.*, Phys. Lett. B **388**, 859 (1996); Phys. Lett. B **420**, 211 (1998); Eur. Phys. J. A **2**, 99 (1998).
[2] R. Bilger *et al.*, Phys. Lett. B **420**, 217 (1998).
[3] S. Sewerin *et al.*, Phys. Rev. Lett. **83**, 682 (1999).
[4] W.K. Eyrich, Prog. Part. Nucl. Phys. **50**, 547 (2003).
[5] P. Kowina *et al.*, Eur. Phys. J. A **22**, 293 (2004).

[6] S. Abd El-Samad *et al.*, Phys. Lett. B **632**, 27 (2006).
[7] Yu. Valdau *et al.*, Phys. Lett. B **652**, 245 (2007).
[8] T. Rożek *et al.*, Phys. Lett. B **643**, 251 (2006).
[9] R.I. Loutitt *et al.*, Phys. Rev. **123**, 1465 (1961).
[10] Yu. Valdau, Ph.D. thesis, University of Cologne (2009), available from `www.fz-juelich.de/ikp/anke/en/theses.shtml`.
[11] R. Siebert *et al.*, Nucl. Phys. A **567**, 819 (1994).
[12] A. Sibirtsev, J. Haidenbauer, H.-W. Hammer, and U.-G. Meißner, Eur. Phys. J. A **32**, 229 (2007).
[13] A. Budzanowski *et al.*, *High resolution study of the* Λp *final state interaction in the reaction* $p+p \to K^+ + (\Lambda p)$, submitted to Phys. Lett. B (2009).
[14] A. Sibirtsev, J. Haidenbauer, H.-W. Hammer, and S. Krewald, Eur. Phys. J. A **27**, 269 (2006).
[15] A. Metzger, Ph.D. thesis, University of Erlangen–Nürnberg (1998); This and Refs. [16–18, 21, 22] are available from `www.fz-juelich.de/ikp/COSY-TOF/publikationen`.
[16] D. Hesselbarth, Ph.D. thesis, University of Bonn (2000).
[17] M. Fritsch, Ph.D. thesis, University of Erlangen–Nürnberg (2002).
[18] W. Schroeder, Ph.D. thesis, University of Erlangen–Nürnberg (2003).
[19] M. Abdel-Bary *et al.*, Phys. Lett. B **595**, 127 (2004).
[20] M. Abdel-Bary *et al.*, Phys. Lett. B **649**, 252 (2007).
[21] L. Karsch, Ph.D. thesis, University of Dresden (2005).
[22] P. Schönmeier, Ph.D. thesis, University of Dresden (2003).
[23] S. Barsov *et al.*, Nucl. Instrum. Methods Phys. Res. Sect. A **462**, 354 (2001).
[24] R. Maier *et al.*, Nucl. Instrum. Methods Phys. Res., Sect. A **390**, 1 (1997).
[25] A. Khoukaz *et al.*, Eur. Phys. J. D **5**, 275 (1999).
[26] M. Büscher *et al.*, Nucl. Instrum. Methods Phys. Res., Sect. A **481**, 378 (2002).
[27] S. Dymov *et al.*, Part. Nucl. Lett. **2**, 40 (2004).
[28] S.N. Dymov *et al.*, Nucl. Instrum. Methods Phys. Res., Sect. A **440**, 431 (2000).
[29] S. Agostinelli *et al.*, Nucl. Instrum. Methods Phys. Res., Sect. A **506**, 250 (2003); `http://geant4.web.cern.ch/geant4`.
[30] C. Amsler *et al.*, Phys. Lett. B **687**, 1 (2008).
[31] A. Baldini, V. Flamino, W.G. Moorhead, and D.R.O. Morison, Landolt-Börnstein, New Series, Ed. H. Schopper (Springer-Verlag, Berlin, 1988).
[32] Cao Xu, Lee Xi-Guo, and Wang Qing-Wu, Chin. Phys. Lett. B **25**, 888 (2008).
[33] Ju-Jun Xie and Bing-Song Zou, Phys. Lett. B **649**, 405 (2007).
[34] T.H. Tan, Phys. Rev. Lett. **23**, 395 (1969).
[35] R.A. Arndt *et al.*, Phys. Rev. C **62** 034005 (2000); solution SP05 `http://gwdac.phys.gwu.edu`.
[36] E. Shikov, Diploma thesis, St. Petersburg State Polytechnical University (2009), available from `www.fz-juelich.de/ikp/anke/en/theses.shtml`.